

RELATIVISTIC JETS AS COMPACT RADIO SOURCES¹

R. D. BLANDFORD AND ARIEH KÖNIGL

W. K. Kellogg Radiation Laboratory, California Institute of Technology

Received 1978 December 26; accepted 1979 March 1

ABSTRACT

Variable extragalactic radio sources, associated with the nuclei of galaxies and quasars, are interpreted in terms of a supersonic relativistic jet. It is proposed that radio emission originates both from the quasi-steady jet itself and from behind strong shock waves which either propagate in the jet, or which are formed behind dense condensations (clouds) that are accelerated to relativistic speeds by the flow. In this way the source could display apparent superluminal expansion in which the moving component (associated with a shock) and the stationary component (associated with the optically-thick core of the jet) would have comparable, Doppler-boosted fluxes. Specific models for the dynamical and radiative properties of the jet and of individual shocks are presented. Kinematical consequences of the relativistic motion are described for flux and polarization measurements, as well as for VLBI observations of superluminal sources. It is argued that the majority of bright compact sources are observed along lines of sight making small ($\lesssim 10^\circ$) angles to the jet velocity. This hypothesis has important consequences for the interpretation of low-frequency variable sources, optically-violent variable quasars, Lacertids, and extended double sources. These are briefly outlined, and some specific observational tests are proposed.

Subject headings: BL Lacertae objects — galaxies: nuclei — quasars —
radio sources: galaxies — radio sources: variable

I. INTRODUCTION

Variable radio emission from active galactic nuclei and quasars is conventionally interpreted as incoherent synchrotron radiation from a nonthermal distribution of relativistic electrons (e.g., Jones, O'Dell, and Stein 1974). For many sources there is no need to question this explanation, but for a sizable fraction of the brighter sources there is ample evidence that simple physical models are inadequate and either must be replaced by more complex models or the synchrotron hypothesis abandoned. The difficulties originate from several types of observation. For some sources, the variability time scales t_{var} are so short that the radio brightness temperatures, based on an estimated source size of ct_{var} , exceed the "inverse Compton" limit of $\sim 10^{12}$ K (e.g., Kellermann and Pauliny-Toth 1969). For some low-frequency variables, temperatures as high as 10^{15} K are derived in this fashion (e.g., Hunstead 1972) and current indications are that this phenomenon is not rare (Condon *et al.* 1978).

VLBI observations of compact sources usually show an elongated radio structure, the position angle of which is roughly fixed and in some cases is related to larger scale radio structure. Apparent superluminal motion of individual components has been measured convincingly in a few cases, and appears to be fairly common among strong sources (Cohen *et al.* 1979). Finally, radio polarization observations in several sources indicate the absence of dynamically significant amounts of thermal plasma (e.g., Wardle 1977; Jones and O'Dell 1977).

These observations strongly suggest the presence of relativistic motion within the emitting region (cf. O'Dell 1978 and references cited therein), and several models (reviewed in Blandford, McKee, and Rees 1977) which incorporate such motion have been investigated. In this paper we describe another general model that we believe has some kinematical, dynamical, and radiative advantages in explaining the data. We suggest that the radio emission originates within a supersonic jet of the type that has been inferred to supply extended radio sources with mass, momentum, and energy (e.g., De Young 1976), and indeed in several cases is directly observed (e.g., Waggett, Warner, and Baldwin 1977; Burch 1977).

The relativistic electrons responsible for the observed synchrotron emission must be accelerated locally within the jet; otherwise, expansion losses would lead to very high total power requirements. One way of achieving this, which is discussed in Blandford and McKee (1977), Jones and Tobin (1977), and Marscher (1978), utilizes strong shock waves. The *mean* electron energy behind a mildly relativistic shock propagating into an electron-proton plasma is likely to be $\gtrsim 100$ MeV, which is adequate to account for the observed radio emission. For this reason, the nonthermal radiative efficiency of the shock can be quite high. The above papers dealt with spherical blast waves and concentrated on the radiative properties of the shocks. In this paper we turn our attention more to the

¹ Supported in part by the National Science Foundation [AST 78-05484, AST 76-80801 A01].

geometrical consequences of assuming that these shocks are confined to a jet. Such shocks could be associated either with dense clouds accelerated by the flow or with an unsteady velocity field in the jet.

In § II we describe some general kinematical consequences of relativistic motion which are relevant to our model. In § III we present an idealized description of the steady radio emission from a relativistic jet, based on a set of simple assumptions. The variable component of the emission, which we associate with shock waves traveling in the jet, is discussed in § IV. Specifically, we examine the dynamical and radiative properties of accelerated clouds and of velocity disturbances which steepen to form propagating shocks. In § V we show that several observed features of compact radio sources can be interpreted on the assumption that these sources are relativistic jets which are viewed at small angles to their axes. In addition, we examine several other consequences of this hypothesis. Our results are summarized in § VI.

II. OBSERVABLE CONSEQUENCES OF RELATIVISTIC MOTION

a) Kinematics

The kinematical consequences of relativistic motion have been described by several authors and are reviewed in Blandford, McKee, and Rees (1977). For a source moving at time t with a space velocity (in units of c) $\beta(t)$ in a direction making an angle θ with the direction of the observer \mathbf{n} , the observed velocity β_{ob} is given by

$$\beta_{\text{ob}} = \frac{\mathbf{n} \times (\beta \times \mathbf{n})}{1 - \beta \cdot \mathbf{n}}. \quad (1)$$

The acceleration of the source is

$$\mathbf{g} = d(\gamma\beta)/dt = \gamma d\beta/dt + \gamma^3(\beta \cdot d\beta/dt)\beta, \quad (2)$$

where $\gamma = (1 - \beta^2)^{-1/2}$. The observed rate of change of β_{ob} is

$$\frac{d\beta_{\text{ob}}}{dt_{\text{ob}}} = (1 - \beta \cdot \mathbf{n})^{-3} [(1 - \beta \cdot \mathbf{n})d\beta/dt + (d\beta/dt \cdot \mathbf{n})(\beta - \mathbf{n})], \quad (3)$$

where t_{ob} is the observer's time. In the case of linear acceleration ($\mathbf{g} \times \beta = 0$), the vector $d\beta_{\text{ob}}/dt_{\text{ob}}$ is collinear with β_{ob} and of magnitude

$$\frac{d\beta_{\text{ob}}}{dt_{\text{ob}}} = \mathcal{D}^3 \sin \theta \mathbf{g}, \quad (4)$$

where \mathcal{D} , the Doppler factor, is given by $\mathcal{D} = \gamma^{-1}(1 - \beta \cdot \mathbf{n})^{-1}$. The maximum value of $d\beta_{\text{ob}}/dt_{\text{ob}}$ is $g \csc^2 \theta$. For a uniform circular motion ($\mathbf{g} \cdot \beta = 0$), \mathcal{D} will be maximized when $\mathbf{g} \cdot \mathbf{n} = 0$, and then

$$d\beta_{\text{ob}}/dt_{\text{ob}} = \gamma \mathcal{D}^2 \mathbf{g}. \quad (5)$$

The Doppler factor can also be written in terms of β_{ob} as

$$\mathcal{D} = (1 - \beta_{\text{ob}}^2 + 2\beta_{\text{ob}} \cot \theta)^{1/2}. \quad (6)$$

For a given value of θ (less than $\pi/2$), \mathcal{D} rises with increasing β_{ob} as $1 + \beta_{\text{ob}} \cot \theta$ for $\beta_{\text{ob}} \ll 1$, reaches a maximum value of $\csc \theta$ at $\beta_{\text{ob}} = \cot \theta$, declines to 1 when $\beta_{\text{ob}} = 2 \cot \theta$, and finally declines to zero as β_{ob} approaches its asymptotic value of $\cot(\theta/2)$.

b) Observed Flux

For a moving source we can relate S_{ob} , the observed flux density, to S , the flux density that would be observed at the same frequency ν in the comoving frame, by

$$S_{\text{ob}}(\nu) = S(\nu) \mathcal{D}^{3+\alpha}, \quad (7)$$

where α is the spectral index ($-d \ln S / d \ln \nu$). (Eq. [7] is true for optically thin sources and spherical optically thick sources. For nonspherical optically thick sources, changes in aspect must be taken into account.) In Figure 1 we plot $S_{\text{ob}}(\beta_{\text{ob}})$ for different viewing angles θ , assuming that $\alpha = 0.5$ and that S is constant. For an accelerating source, the flux will at first rise until $\beta = \cos \theta$, and then decline as the emitted radiation is beamed away from the observer direction.

For a narrow stationary cylindrical jet, however, it is the observed surface brightness Σ_{ob} that is important. For an optically thin source, this is related to the surface brightness Σ_{\perp} that would be measured by a comoving observer whose line of sight was perpendicular to the jet velocity by

$$\Sigma_{\text{ob}}(\nu) = \Sigma_{\perp}(\nu) \mathcal{D}^{(2+\alpha)} \csc \theta. \quad (8)$$

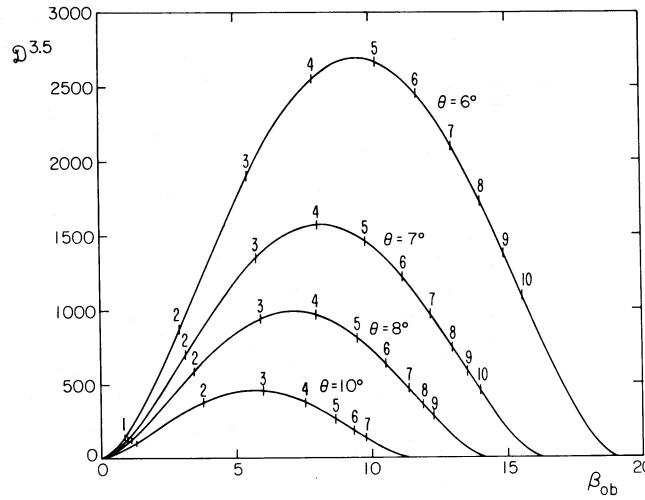


FIG. 1.—The observed flux density S_{ob} from a moving source as a function of the observed velocity β_{ob} , under the assumption that in the frame of the source the flux is constant and has spectral index $\alpha = 0.5$. The curves are distinguished by different values of θ , the angle in the observer's frame between the direction of motion and the line of sight. The tick marks on each curve indicate values of the proper velocity $\gamma\beta$.

If a source combines parts moving with different speeds, then according to both equations (7) and (8) a distant observer will see predominantly those parts that are moving with $\beta \sim \cos \theta$, for which the Doppler factor \mathcal{D} is maximized.

c) Flux Variation

The observed flux from a relativistically moving source can vary either kinematically or as a consequence of intrinsic variability in the comoving flux S . Differentiating equation (7), we obtain

$$\delta \ln S_{\text{ob}} = \delta \ln S + (3 + \alpha) \left\{ \left(\frac{\mathcal{D} - \gamma}{\gamma\beta^2} \right) \delta \ln \gamma + \gamma\beta\mathcal{D}\delta \cos \theta \right\}. \quad (9)$$

In the small-angle, ultrarelativistic approximation, this becomes

$$\delta \ln S_{\text{ob}} = \delta \ln S + \frac{(3 + \alpha)}{(1 + \gamma^2\theta^2)} [(1 - \gamma^2\theta^2)\delta \ln \gamma - 2\gamma^2\theta\delta\theta]. \quad (10)$$

In this limit, it is the third term associated with curvature in the trajectory that is most likely to dominate the variation.

d) Observer-Averaged Mean Flux

If an observed compact radio source comprises several rapidly moving components, then we must use the observer time-average for the mean flux. If similar radio sources are formed at a rate R with a constant intrinsic flux S and move with a fixed velocity β out to some fixed radius r_d (roughly the length scale for decay of the flux), then the mean observed flux will be given by

$$\bar{S}_{\text{ob}} = \mathcal{D}^{(3+\alpha)}(1 - \beta \cos \theta)R(r_d/\beta c)S. \quad (11)$$

Alternatively, if each source has an acceleration $g(\gamma\beta)$, then the observed flux will peak when β is closest to $\cos \theta$. For linear acceleration, the mean observed flux will be given by

$$\bar{S}_{\text{ob}} = \int d\beta RSg^{-1}\gamma^2\mathcal{D}^{2+\alpha}. \quad (12)$$

For uniform circular motion,

$$\bar{S}_{\text{ob}} = \int d\chi RS\beta g^{-1}\mathcal{D}^{2+\alpha}, \quad (13)$$

where χ , the orbital phase, is related to θ and θ_0 , the inclination of the orbital plane, through $\cos \theta = \cos \theta_0 \cos \chi$.

The integrals in equations (12) and (13) are elementary if S and g are constant (a fair approximation for small θ) and $\alpha = 0$. Assuming that the linearly accelerating source radiates for $0 \leq \beta \leq \beta_1$, we obtain

$$\bar{S}_{ob} = RSg^{-1}\beta_1(1 - \beta_1 \cos \theta)^{-1}. \tag{14}$$

Likewise, for a circularly accelerating source radiating for a single revolution,

$$\bar{S}_{ob} = 2\pi RSg^{-1}\gamma^{-2}\beta(1 - \beta^2 \cos^2 \theta_0)^{-3/2}. \tag{15}$$

More generally, for $\theta, \theta_0 \gtrsim \gamma^{-1}$, equations (12) and (13) can be approximated by $\bar{S}_{ob} \sim RSg^{-1}(\theta)\theta^{-(2+\alpha)}$ and $\bar{S}_{ob} \sim RSg^{-1}(\theta_0)\theta_0^{-(1+\alpha)}$, respectively. One important corollary follows from these expressions. Suppose that the sources have roughly the same constant acceleration and intrinsic fluxes, and that their velocities are contained within a finite range of solid angles that includes the observer direction \mathbf{n} . Then if $\alpha > 0$, the *mean* observed power will be dominated, for both linear and circular accelerations, by those sources moving with $\theta \lesssim \gamma^{-1}$. The background flux arising from sources that have $\theta \gg \gamma^{-1}$ can generally be ignored. This argument is relevant to our interpretation of sources which are confined to two antiparallel jets (see § V).

e) Polarization

A further important feature of the radiation observed from an accelerating source is the characteristic swing in the polarization position angle.

We consider first the case of collinear acceleration. Suppose that the magnetic field \mathbf{B} in the source is uniform and its observed direction is specified by the angles (η, ψ) , as defined in Figure 2a. If the radiation is produced by the synchrotron process, then the electric vector \mathbf{e} in the comoving frame will be normal to the magnetic field direction (as well as to the emission direction \mathbf{k}). We can thus use the fact that the Lorentz invariant $\mathbf{e} \cdot \mathbf{B} = 0$ to solve for the observed position angle ξ . A straightforward calculation yields

$$\tan \xi = \frac{\cos \psi [\beta - \cos \theta (1 - \tan \psi \tan \theta)]}{\tan \eta (\beta \cos \theta - 1)}, \tag{16}$$

where βc is the velocity of the source and θ is the angle between β and the observer direction \mathbf{n} . The dependence of ξ on β is due to the fact that, as β changes, so does the aberration angle (the angle between \mathbf{k} and \mathbf{n}), and that \mathbf{e} must remain normal to \mathbf{k} .

We shall be most interested in the limit $\psi, \theta \ll 1, \beta \rightarrow 1$, appropriate for a relativistic source with magnetic field roughly perpendicular to its velocity (see § V). According to equation (16), ξ will then swing very rapidly from a

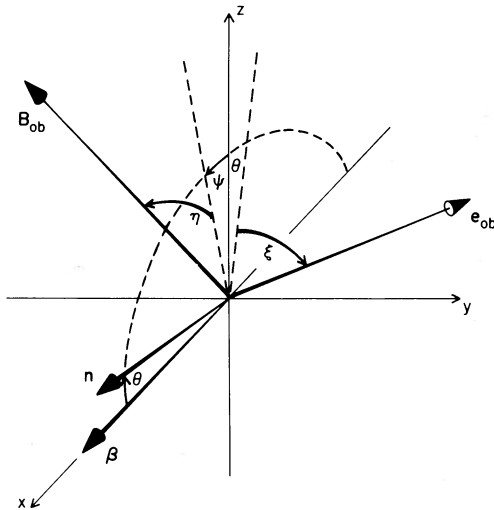


FIG. 2a

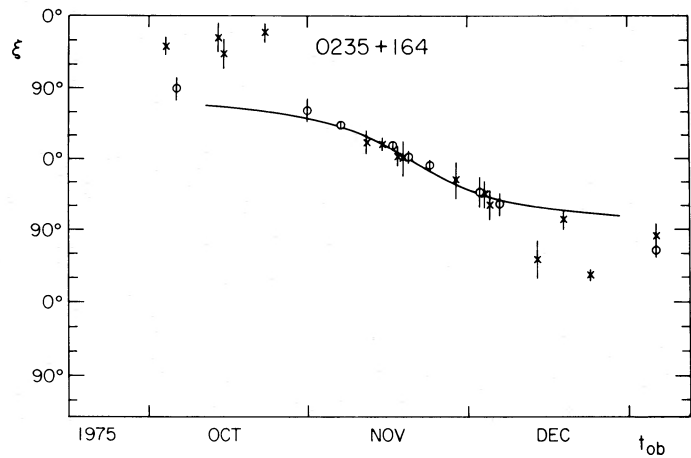


FIG. 2b

FIG. 2.—(a) Geometry of the emission region, which moves with a velocity β , as seen in a stationary frame. Synchrotron radiation (electric field \mathbf{e}_{ob}) is emitted by relativistic electrons which move in a static magnetic field \mathbf{B}_{ob} . The vector \mathbf{e}_{ob} (\mathbf{B}_{ob}) makes an angle ξ (η) with the plane containing β and the observer direction \mathbf{n} , and its projection on this plane makes an angle θ (ψ) with the z axis. (b) The observed polarization position-angle ξ in the 1975 outburst of AO 0235+164 (reproduced from Ledden and Aller 1978). The measurements were made at 8.0(0) and at 14.5(x) GHz, with standard errors as shown. The solid line represents a fit to the data in the accelerating-cloud model of § IV, for a cloud with acceleration parameter $a = 100$ which starts from rest at a distance $r_0 = 10$ pc from the origin of a paraboloidal jet with a constant Lorentz factor $\gamma_j = 10$. The values of θ, ψ , and η which give rise to this curve are not unique. One possible choice is $\theta = 5^\circ, \psi = 15^\circ$, and $\eta = 5^\circ$.

constant value $\xi \sim (\pi/2 - \eta)$ to a constant value $\xi \sim (\eta - \pi/2)$ when $\beta \sim (\cos \theta - \sin \theta \tan \psi)$. For a given value of the viewing angle θ , the velocity at which the swing occurs depends rather sensitively on ψ , whereas the amplitude of the swing is determined primarily by η . The maximum observable amplitude of the swing is 180° . A specific example of this phenomenon in an accelerating source is shown in Figure 2*b* and discussed in § V. (Sources decelerating from relativistic speeds would exhibit similar polarization swings.)

For a uniform circular motion (described by the angles θ_0, χ as before), we can assume either that the magnetic field direction is fixed in space or that it is convected with a constant orientation with respect to β . In the former case,

$$\tan \xi = \frac{\cos \psi [\beta \cos \chi - \cos \theta_0 (1 - \tan \theta_0 \tan \psi)]}{\tan \eta [\beta \cos \chi \cos \theta_0 - 1] + \beta \sin \chi \sin (\theta_0 + \psi)}, \quad (17)$$

and the swing in position angle is similar to that given by equation (16). For a convected field,

$$\tan \xi = \frac{\cos \psi_0 [\beta \cos \chi - \cos \theta_0 (1 - \tan \theta_0 \tan \psi_0 \cos \chi)] + \sin \theta_0 \tan \eta_0 \sin \chi}{\tan \eta_0 (\beta \cos \theta_0 - \cos \chi) + \sin \chi (\sin \psi_0 + \beta \cos \psi_0 \sin \theta_0)} \quad (18)$$

(where η_0 and ψ_0 are the respective values of η and ψ at $\chi = 0$), and the observed polarization position angle behaves rather differently. In the limit $\gamma^{-1} \ll \theta_0, \psi_0 \ll 1$, the effects of convection and aberration will cancel each other, and ξ will have an approximately constant value of $\sim (\eta - \pi/2)$ when the source is bright. Both types of magnetic field behavior could occur in realistic source geometries. Related formulae for the polarization swing in circular motion have been given by Ferguson (1971).

III. RADIO EMISSION FROM A STEADY JET

a) Jet Properties

In this section we present an idealized model of a steady radio jet. This allows us to quantify our discussion and derive expressions for observable quantities. We consider a narrow conical jet of small semiangle φ whose axis makes an angle θ with the direction of the observer (the observed opening angle is $\phi_{\text{ob}} = \phi \csc \theta$). We assume that the jet is supersonic and free, and that it has a constant velocity β_j . The jet convects a tangled magnetic field B (measured in the frame of the fluid) which will vary as r^{-1} , where r is the distance from the apex (cf. the model of NGC 6251 in Readhead, Cohen, and Blandford 1978). We assume that relativistic electrons can be accelerated continuously within the jet, and that their distribution function is $N(\gamma_e) = K\gamma_e^{-2}$, with $\gamma_{e\text{min}} < \gamma_e < \gamma_{e\text{max}}$ and $\gamma_{e\text{max}} \gg \gamma_{e\text{min}}$. These electrons will radiate synchrotron radiation with a spectral index $\alpha = \frac{1}{2}$. The electron energy density $u_e = K\Lambda m_e c^2$ [with $\Lambda = \ln(\gamma_{e\text{max}}/\gamma_{e\text{min}})$] is insensitive to the exact values of $\gamma_{e\text{min}}$ and $\gamma_{e\text{max}}$, and we assume approximate equipartition with the magnetic energy density,

$$u_e = k_e \Lambda B^2 / 8\pi, \quad (19)$$

where k_e is a constant $\lesssim 1$. This implies that the effective Mach number \mathcal{M} of the jet (the ratio of its proper velocity to the proper speed of sound) is constant. If the electrons (mass m_e) are neutralized by protons (mass m_p) exerting a negligible pressure, then

$$\mathcal{M} \sim [\gamma_{e\text{min}}(m_e/m_p)(\Lambda/3 + 1/k_e)]^{-1/2} \gamma_j \beta_j, \quad 1 \ll \gamma_{e\text{min}} \ll (m_p/m_e). \quad (20)$$

A free jet would have $\phi \gtrsim \mathcal{M}^{-1}$; but if $\gamma_{e\text{min}} \sim 10\text{--}100$, as indicated by Faraday rotation measurements (e.g., Wardle 1977), then we expect that $\phi \lesssim \gamma_j^{-1}$. This relation should also hold in the case of a relativistic electron-positron plasma (for which $\mathcal{M} \sim \gamma_j \beta_j$) if γ_j is large.

b) Radiative Properties

An important consequence of the equipartition assumption is that the relativistic electrons must remain roughly isothermal, as the particle density and internal energy density both decay as r^{-2} . There must then be ongoing particle acceleration to compensate for the cooling associated with adiabatic decompression in the expanding jet. An estimate of the upper cutoff in the electron distribution function $\gamma_{e\text{max}}$ can be obtained by equating the synchrotron cooling time $t_s \sim 3 \times 10^7 \gamma_j \mathcal{D}_j^{1/2} v_0^{-1/2} B^{-3/2}$ s to the expansion time $\sim 1 \times 10^8 r_{\text{ob}} \csc \theta \beta_j^{-1}$ s, which should be comparable to the reacceleration time scale of the relativistic electrons. Here \mathcal{D}_j is the Doppler factor of the jet, v is measured in GHz, B is measured in gauss, and $r_{\text{ob}} = r \sin \theta$, the observed radius, is measured in parsecs. The observed optically thin spectrum from r_{ob} should thus have a slope of $\alpha = 0.5$ up to the frequency

$$\nu_{u9}(r_{\text{ob}}) = 0.07(1+z)^{-1} \gamma_j^2 \beta_j^2 \mathcal{D}_j \csc \theta B_1^{-3} r_{\text{ob}}, \quad (21)$$

which is the characteristic emission frequency of an electron with Lorentz factor $\gamma_{e\text{max}}$ (z is the redshift of the source, and the subscript 1 indicates a quantity measured at $r = 1$ pc). Provided that the injected electron distribution

function has the same slope for $\gamma_e \gtrsim \gamma_{e\max}$, then the local radiation spectrum would steepen at frequencies $\nu > \nu_u$ to $\alpha \sim 1$, as a result of synchrotron losses (cf. Kellermann 1966). If the emission region extends from r_{\min} to r_{\max} , then, apart from some model-dependent geometrical and spectral factors of order unity, the total synchrotron power radiated by the jet is

$$L_s \approx \frac{1}{2}k_e(1 + \frac{2}{3}k_e\Lambda)^{-1}L, \quad (22)$$

where $L = 10^{44}L_{44}$ ergs s⁻¹ is the total power carried by the jet in the form of relativistic electrons and magnetic field, and is given by

$$L \approx \frac{1}{4}\Delta(1 + \frac{2}{3}k_e\Lambda)\gamma_j^2\beta_j c B^2 r^2 \phi^2, \quad (23)$$

where $\Delta = \ln(r_{\max}/r_{\min})$. (We assume that other contributions to the internal power in the jet can be ignored.) The jet is therefore a fairly efficient radiator, in which the radiated energy is constantly replenished by dissipation of the bulk kinetic energy. Indeed, we expect that γ_j would decline slowly with r . In addition, the ratio of the comoving synchrotron-radiation energy density to the magnetic energy density is constant and given by

$$u_s/(B^2/8\pi) \sim k_e\beta_j\gamma_j\phi. \quad (24)$$

If, as we expect, $\gamma_j \leq \phi^{-1}$ in the strongest observed sources, then equation (24) implies that the Compton power will not exceed the synchrotron power. In fact, if γ_j were much greater than ϕ^{-1} , then the Compton losses would probably be so severe as to decelerate the jet until $\gamma_j \sim \phi^{-1}$.

The brightness temperature in the comoving frame will not greatly differ from the critical value of $T' \sim 10^{12}$ K (e.g., Kellermann and Pauliny-Toth 1969). The observed brightness temperature can be calculated using equation (8). In our model,

$$T(\nu, r) \approx 3 \times 10^{10}(1+z)^{-1/2}\nu_9^{1/2}B_1^{-1/2}\mathcal{D}_j^{1/2}r_{\text{ob}}^{1/2}(\sin\theta)^{-1/2}(1-e^{-\tau}) \text{ K}, \quad (25)$$

where τ is the optical depth to synchrotron self-absorption which, for a line of sight through the jet that passes at a distance d from the jet axis, is given by

$$\tau(\nu, r) \approx 500(1+z)^{-3}K_1B_1^2\nu_9^{-3}\mathcal{D}_j^2\sin^2\theta(\phi^2 - \delta^2)^{1/2}r_{\text{ob}}^{-3}, \quad 0 \leq \delta = \tan^{-1}(d/r) \leq \phi. \quad (26)$$

Differentiating equation (25) with respect to r and substituting equations (19), (21), and (23), we find that the brightness temperature has a maximum value, *independent of frequency*, of

$$T_{\max} = \mathcal{D}_j(1+z)^{-1}T'_{\max} \approx 3 \times 10^{11}(1+z)^{-1}k_e^{1/6}(1 + \frac{2}{3}k_e\Lambda)^{-1/12} \\ \times \Delta^{-1/12}\gamma_j^{-1/6}\beta_j^{-1/12}\mathcal{D}_j^{5/6}(\sin\theta)^{-1/3}\phi_{\text{ob}}^{-1/6}L_{44}^{1/12} \text{ K} \quad (27)$$

on the jet axis ($\delta = 0$), at a projected radius of

$$r_{\text{maxob}} \approx 3(1+z)^{-1}k_e^{1/3}\Delta^{-2/3}(1 + \frac{2}{3}k_e\Lambda)^{-2/3}\gamma_j^{-4/3}\beta_j^{-2/3}\mathcal{D}_j^{2/3}(\sin\theta)^{-1/3}\phi_{\text{ob}}^{-1}L_{44}^{2/3}\nu_9^{-1}. \quad (28)$$

Note that, apart from the Doppler factor, equation (27) is very insensitive to the jet parameters. Since, for a given baseline, the angular resolution of a VLBI measurement is proportional to the observed wavelength, the fact that $r_{\text{obmax}} \propto \nu^{-1}$ indicates that if the "core" of the jet appears to be unresolved at a given frequency, it will remain so at other frequencies.

The observed flux $S_{\text{ob}} \propto \nu^2 r_{\text{obmax}}^2 T_{\max}$ is also independent of frequency, and so the jet will appear to have a flat spectrum of flux density

$$S_{\text{ob}} \approx 0.5(1+z)k_e^{5/6}\Delta^{-17/12}(1 + \frac{2}{3}k_e\Lambda)^{-17/12}\gamma_j^{-17/6}\beta_j^{-17/12}\mathcal{D}_j^{13/6}(\sin\theta)^{-5/6}\phi_{\text{ob}}^{-1}L_{44}^{17/12}D_{19}^{-2}J_y, \quad (29)$$

where D_{19} Gpc is the *luminosity* distance to the source. The spectrum will be flat up to the frequency ν_b , the upper cutoff frequency ν_u of the electron energy distribution evaluated at the radius r_b , where the maximum brightness temperature is achieved. Combining equations (21) and (28), we obtain (for $\delta = 0$)

$$\nu_{b9} \approx 60(1+z)^{-1}k_e^{1/6}\Delta^{5/12}(1 + \frac{2}{3}k_e\Lambda)^{5/12}\gamma_j^{11/6}\beta_j^{17/12}\mathcal{D}_j^{5/6}(\sin\theta)^{5/6}\phi_{\text{ob}}L_{44}^{-5/12} \quad (30)$$

and

$$r_{b\text{ob}} \approx 0.04k_e^{1/6}\Delta^{-13/12}(1 + \frac{2}{3}k_e\Lambda)^{-13/12}\gamma_j^{-19/6}\beta_j^{-25/12}\mathcal{D}_j^{-1/6}(\sin\theta)^{-7/6}\phi_{\text{ob}}^{-2}L_{44}^{13/12}. \quad (31)$$

For $\nu > \nu_b$ the spectrum will be dominated by the contribution from $r \lesssim r_b$ and will steepen to $\alpha \sim 1$ (again, as a consequence of synchrotron losses). The detailed high-frequency spectrum depends on the efficiency of the particle acceleration in the innermost parts of the jet.

c) Polarization

The degree of polarization of the synchrotron radiation from the jet reflects the degree of order in the magnetic field. The magnetic field law $B \propto r^{-1}$ refers in fact only to the transverse component, whereas the parallel component scales as $B_{\parallel} \propto r^{-2}$. However, only a small degree of shear in the flow is necessary to isotropize the field. The degree of polarization should be higher at optical wavelengths than at radio wavelengths, because for $\nu > \nu_b$ the jet is optically thin, and also because the magnetic field will presumably maintain a higher degree of order over the smaller emission region ($r \lesssim r_b$) of the optical radiation. The observed position angle is more difficult to interpret, especially if the angle θ is small, as we suggest below, and projection effects become important. Furthermore, as the emission at different frequencies originates from different radii, both the degree and the direction of intrinsic polarization may vary with radio frequency.

We can, however, estimate the Faraday rotation across the jet. This is probably dominated by the lowest energy relativistic electrons (Wardle 1977; Jones and O'Dell 1977). As long as the electron distribution function remains unchanged, the rotation $\Delta\Phi \propto KB\nu^{-2}r$ evaluated at $r_{\max}(\nu)$ is also independent of frequency, and is given (for $\delta = 0$) by

$$\Delta\Phi[r_{\max}(\nu)] \approx 4 \times 10^4 k_e^{1/3} \Delta^{-1/6} (1 + \frac{2}{3} k_e \Lambda)^{-1/6} \gamma_j^{-1/3} \beta_j^{-1/6} \mathcal{D}_j^{-1/3} (\sin \theta)^{-1/3} L_{44}^{1/6} F \text{ rad}, \quad (32)$$

where F is a factor determined by the shape of the distribution function near $\gamma_{e \min}$. For a finite power law,

$$F \sim \gamma_{e \min}^{-3} \ln(\gamma_{e \min}) \quad (33)$$

(Wardle 1977). Equation (32) represents an upper bound for $\Delta\Phi$ in the optically thin regions of the jet, which can be reduced if there is small-scale disorder in the field. For a relativistic electron-positron plasma, the Faraday rotation will be zero, although the effects of repolarization may be observable.

Equations (27)–(32) are the principal results of our study of this model and allow the parameters of the jet to be estimated using observed quantities. (However, they may also apply to other models which do not involve jets.) In deriving these expressions, we have combined some fairly common assumptions, such as flux freezing and equipartition, with a few rather specific postulates (constant γ_j and φ , emission spectrum with $\alpha = 0.5$) in order to make the model as simple as possible. In § V we apply these estimates to the source 3C 345.

IV. RADIO VARIABILITY

In the previous section we showed how steady radio emission may originate from a relativistic jet. Compact radio sources, however, are characterized by variability in both their total flux and radio structure. In this section we describe two mechanisms whereby time-dependent phenomena can arise—the acceleration of clouds, and the propagation of shocks within the jet.

a) Dynamics of a Cloud

If we immerse a small, dense blob of gas in a rapidly moving jet, it will quickly come into rough pressure equilibrium with its surroundings, and form a cloud of mass M and internal energy E_0 . (The subscript zero will be used to denote the initial parameters of the cloud.) The cloud will then be accelerated by the jet and expand as it moves downstream. We shall assume that the expansion is adiabatic with a specific heat ratio $\Gamma = 5/3$ (the generalization to a relativistic equation of state is straightforward; cf. Christiansen, Scott, and Vestrand 1978). The equations governing the acceleration and expansion of the cloud are

$$Mg = Mcd(\gamma\beta)/dt = k_a p_a h^2, \quad (34)$$

$$p_a = k_b \gamma^2 (\beta_j - \beta)^2 \omega_j, \quad (35)$$

$$E = k_c Mgh = E_0 (h/h_0)^{-2} \quad (36)$$

(cf. Blandford and Königl 1979). Here γ and βc are the Lorentz factor and velocity of the cloud, respectively, and h , the scale height of the cloud, is defined by $h = p_a / \rho_a g$ (where p_a and ρ_a are the pressure and rest mass density of the cloud at its upstream end); ω_j is the enthalpy density in the jet. In the model of § III, $\omega_j \sim Km_p c^2 / \gamma_{e \min}$ for a plasma dominated by the inertia of cold protons, whereas $\omega_j \sim [(4/3)K\Lambda m_e c^2 + B^2/4\pi]$ for a relativistic electron-positron plasma. In this section we allow the cross-sectional area A of the jet to increase as an arbitrary power of the radius, $A \propto r^n$ ($n = 2$ gives a conical jet which may be free; $n = 1$ corresponds to a paraboloidal jet which requires transverse pressure support). We assume that the speed of the jet is highly supersonic with respect to the cloud, in which case a strong standing bow shock will form upstream from the cloud (cf. Blandford and Königl 1979). The quantities k_a , k_b , and k_c are constants fixed by detailed assumptions about the nature of the shock and of the cloud; k_b may be estimated by imposing the continuity conditions for the energy and momentum fluxes across the shock in the frame of the cloud, and assuming that behind the shock the fluid flows adiabatically with a specific heat ratio $\Gamma = 4/3$. With these assumptions $k_b = 0.84$. (For comparison, $k_b = 0.88$ in the Newtonian

limit.) In addition, we adopt for the cloud the isothermal model of De Young and Axford (1967), for which $k_a = (\pi/2)(\pi^2 - 4) = 9.2$ and $k_c = 1.5$.

We now specialize to an ultrarelativistic jet with constant velocity $\beta_j \sim 1$. For a cloud starting from rest at r_0 , the equation of motion is

$$\left(\frac{1 + \beta}{1 - \beta}\right)^{3/5} \beta \frac{d(\gamma\beta)}{dx} = ax^{-3n/5}, \quad (37)$$

where $x = r/r_0$ and

$$a = \frac{k_a k_b r_0 h_0^2 \gamma_j^2 \omega_j}{Mc^2} = 4.4 \times 10^{-2} k_d r_0 L_{44} M^{-1} (h_0^2/A_0), \quad (38)$$

measuring r_0 in parsecs and M in M_\odot ; k_d is a constant which, in the model of § III, equals $(k_e/\gamma_{e \min})(m_p/m_e)\{\Delta[2 + (4/3)k_e\Lambda]\}^{-1}$ for an electron-proton plasma, and Δ^{-1} for an electron-positron plasma. Equation (37) has the approximate solution

$$\begin{aligned} \gamma\beta &\approx \left[\frac{10a}{5-3n} (x^{(5-3n)/5} - 1) \right]^{1/2} && \text{for } \gamma\beta \ll 1 \\ &\approx \left[2^{-6/5} \frac{11a}{5-3n} (x^{(5-3n)/5} - 1) \right]^{5/11} && \text{for } \gamma\beta \gg 1. \end{aligned} \quad (39)$$

Thus, if the channel area increases more rapidly with radius than $r^{5/3}$, as it does when the jet expands freely, then the cloud will not attain the jet velocity, but will instead approach a smaller maximum speed determined by the acceleration parameter a . If $n < 5/3$, the momentum flux falls sufficiently slowly with r that the cloud will eventually be accelerated to $\beta \sim \beta_j$ for any value of a . The acceleration g is always largest close to r_0 , which is probably much smaller than the radius at which the source is observed. In this case no significant acceleration would be observed for $n > 5/3$, and for $n < 5/3$ we can apply equation (4) when the source is brightest (i.e., when $\beta_{\text{ob}} = \csc \theta = \gamma = \mathcal{D}$) to obtain

$$\frac{d \ln(\beta_{\text{ob}})}{d \ln(r_{\text{ob}})} \approx \left(\frac{5-3n}{11} \right), \quad n < 5/3. \quad (40)$$

The scale height h evolves according to

$$h = h_0 x^{n/5} \gamma^{-2/5} (1 - \beta/\beta_j)^{-2/5}, \quad (41)$$

and increases with x . In the ultrarelativistic case considered here, $h \propto x^{(2+n)/11}$ for $n < 5/3$ and $x \gg 1$; the requirement that h increase slower than the jet width then implies $n > 4/9$. The solution of equation (37) can be integrated once more (numerically) to obtain $x(t)$. The general features of the motion do not seem to be particularly sensitive to our assumptions, unless inhomogeneity in the jet causes the cloud to be deflected through an angle $\delta\theta \gtrsim \gamma^{-1}$ (cf. Christiansen and Scott 1977).

b) Radiative Properties

A large fraction of the bulk kinetic energy flux in the jet which is incident upon the cloud will be dissipated in the strong bow shock, and some of this energy may appear in relativistic electrons behind the shock. In addition, if the jet carries a frozen-in magnetic field, it will be amplified behind the shock. This is therefore a likely site for synchrotron and inverse-Compton radiation (cf. Blandford and McKee 1977; Jones and Tobin 1977). The nature of the flux variations that would be observed from a cloud accelerating according to equations (34)–(36) is illustrated in Figure 3 for a paraboloidal jet ($n = 1$). The observed time evolution of the flux is plotted for two different radiative assumptions:

i) The power radiated in the frame of the cloud is proportional to the rate of dissipation of jet kinetic energy in the frame of the shock, and the spectrum extends up to a fixed maximum frequency with $\alpha = 0.5$, i.e.,

$$S_{\text{ob}}(\nu) \propto \mathcal{D}^{3.5} g \left(\frac{\beta_j - \beta}{1 - \beta\beta_j} \right). \quad (42)$$

(We are assuming that the radiation is emitted in a frame which moves with the velocity of the cloud, although in practice the relevant velocity will be somewhat greater than β .)

ii) As in § III, we assume that the electrons behind the shock have a power-law energy distribution $N(\gamma_e) = K\gamma_e^{-2}$, and emit synchrotron radiation in an equipartition magnetic field, i.e., $K \propto B^2 \propto p_a$. The cloud may initially be optically thick due to synchrotron self-absorption, but the optical depth τ decreases as the cloud expands.

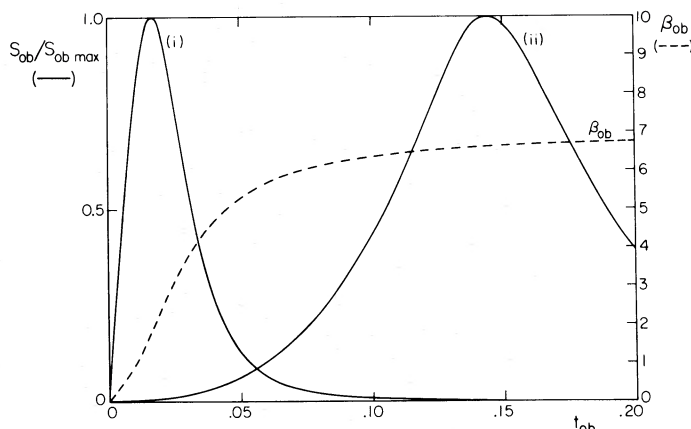


FIG. 3.—The observed flux density (normalized by $S_{\text{obs max}}$) from an accelerating cloud as a function of the observer's time t_{ob} , measured in units of r_0/c . [For a cloud which has been accelerated from r_0 to r in time t , $t_{\text{ob}} = t - (r - r_0) \cos \theta/c$.] The curves labeled (i) and (ii) correspond to the two radiative assumptions discussed in the text; in case (ii) the cloud is initially optically thick, with optical depth $\tau_0 = 10^7$. Also shown is the time evolution of the observed velocity β_{ob} . In this example the jet is paraboloidal with $\gamma_1 = 7$, the acceleration parameter $a = 90$, and the jet is viewed at an angle $\theta = 8^\circ$ to its axis.

Also plotted in Figure 3 is the observed velocity β_{ob} (eq. [1]) as a function of t_{ob} . In order for superluminal motion to be observed, it is necessary that the flux remain appreciable when high values of β_{ob} are attained. This condition is not fulfilled in case (i), where the flux peaks at relatively small values of β_{ob} , and then declines rapidly with decreasing acceleration. In case (ii), however, the peak in the flux occurs when $\tau \sim 1$, and may be reached at large values of β_{ob} if the source is initially opaque with $\tau_0 \gg 1$.

c) Origin of the Clouds

The clouds that we envision are much denser than the jet and smaller than the jet's width ($h_0 < A_0^{1/2}$). Their sizes are also limited by the requirement that, as measured in the cloud frame, the time scale for pressure equilibration [$\sim (h/g)^{1/2}$] be much smaller than either the acceleration time scale ($\sim \beta c/g$) or the travel time [$\sim (r - r_0)/\gamma \beta c$]. However, the clouds should be large enough to form effective obstacles in the jet. The type of astronomical object which satisfies these requirements depends on the physical conditions in the jet at a distance $\lesssim 1$ pc from its origin, where we expect the clouds to be formed.

One plausible class of objects may be associated with emission-line filaments. Most quasars and Seyfert 1 galaxies exhibit broad emission lines in their spectra. These are generally interpreted as originating in dense ($\sim 10^{-15}$ g cm $^{-3}$), photoionized clouds. General arguments (e.g., Osterbrock 1978) indicate that these clouds are located at a distance $r_0 \sim 0.3$ pc from the central continuum source and move coherently with a velocity $v \sim 10^4$ km s $^{-1}$. (However, if the optical continuum is itself beamed, r_0 may be smaller.)

If a cloud of size h_0 enters the jet with a transverse speed v_\perp , it will fragment while entering the flow unless v_\perp is large enough, but will leave the opposite side of the jet before being accelerated by the flow if v_\perp is too large. This implies that

$$(g_0 h_0)^{1/2} \lesssim v_\perp \lesssim (g_0 r_0)^{1/2} \varphi. \quad (43)$$

Adopting the standard cloud parameters quoted above, and estimating g_0 with equation (38) using $k_a = 1$, these inequalities become

$$(h_0/10^{13} \text{ cm}) \lesssim L_{44} \lesssim 10^5 \varphi^2. \quad (44)$$

Conditions (44) will generally be satisfied by clouds of size $h_0 \sim 10^{13}$ – 10^{15} cm, which is consistent with the range that is indicated by independent arguments (e.g., Shields 1978).

As discussed in Blandford and Königl (1979), supernova explosions provide an alternative source of clouds. It is difficult to assess the likelihood of this happening within a jet; but if the explosion involves an energy $U = 10^{51} U_{51}$ ergs, then the ejecta will expand to a radius $\sim 10^{17} U_{51}^{1/3} L_{44}^{-1/3} A_{034}^{1/3}$ cm before being stopped by the impact with the jet. Large nova explosions with energies $\sim 10^{48}$ ergs may likewise give rise to clouds which, if formed sufficiently close to the origin of the jet, will block a significant fraction of its width.

d) Propagation of Shocks in a Relativistic Jet

An alternative source of radio variability is non-steady motion within the jet itself. Dissipative behavior close to the origin, resulting perhaps from surface instabilities, may lead to fluctuations in the radial velocity. Even if

the amplitude of these disturbances is initially small, they may steepen and form shocks farther out in the jet (Rees 1978). A sufficiently strong shock could appear to a distant observer like a separate radio component moving with a Lorentz factor $\gamma \gtrsim \gamma_j$. The Lorentz factor γ_1 of the emitting material behind the shock remains close to γ ; in fact, $\gamma_1 = \gamma/\sqrt{2}$ for $\gamma \gg \gamma_j$, and becomes comparable to γ when γ approaches γ_j . The kinematical and radiative properties of the shock will thus be similar to those of a cloud moving with a Lorentz factor γ . For an electron-proton plasma, the mean Lorentz factor $\bar{\gamma}_e$ associated with the random electron motion behind the shock can be estimated in the limit $\gamma_j \gg 1$ as

$$\bar{\gamma}_e \sim \frac{500(\gamma^2 - \gamma_j^2)^2}{(\gamma^2 + \gamma_j^2)\gamma\gamma_j} \quad (45)$$

(Blandford and McKee 1977). Thus, as the shock weakens and γ approaches γ_j , the accelerated electrons will have the sub-GeV energies implied from radio observations. However, if the bulk motion is relativistic, the emission will still be beamed with a high Doppler factor, which will then in fact be comparable with the Doppler factor of the steady emission from the jet.

It may be possible to discriminate observationally (with VLBI) between the accelerating cloud and propagating shock models by searching for an asymmetry in the brightness distribution of moving radio components. Accelerating clouds should have the steepest radio contours facing the nuclear core, whereas the reverse should hold for propagating shocks, as well as for decelerating clouds (c.f. Christiansen, Scott, and Vestrand 1978). Furthermore, it may even be possible for the acceleration or the deceleration to be directly observable (cf. eqs. [3]–[5] and [40]).

In § III we postulated that the relativistic electrons are able to remain effectively isothermal in the expanding jet. This may conceivably be achieved by weak shocks and fluid turbulence associated with noise in the jet. The details of these processes will be discussed elsewhere.

V. COMPACT RADIO SOURCES

a) Radio Flux

Compact radio sources (i.e., those whose flux at an intermediate radio frequency, e.g., ~ 1 GHz, is dominated by the contribution of a single bright component smaller than ~ 1 kpc in size) usually exhibit flat radio spectra and radio variability (e.g., Brandie, Bridle, and Kesteven 1974). In addition, the ratio of optical to radio power tends to be higher in these objects than in steep-spectrum sources (e.g., Usher 1975), making identification easier (e.g., Condon, Balonek, and Jauncey 1975). Flat-spectrum radio sources are nearly always associated with quasars (Wall 1975), although only $\sim 5\%$ of quasars are radio-loud (e.g., Sramek and Weedman 1978).

The fluxes at high (i.e., $\gtrsim 1$ GHz) radio frequencies seem to vary on time scales roughly proportional to the wavelength, indicating the presence of a constant ($\sim 10^{12}$ K) brightness temperature (e.g., O'Dell 1978). This temperature, which is confirmed by VLBI measurements, is generally slightly greater than the inverse Compton limit for a nonrelativistic source. In § III we have described the radio properties of a simple model of a steady jet. We have found that if we make simple but natural assumptions about the magnetic field and relativistic electron distribution function, then the source inhomogeneity leads to a flat spectrum and constant temperature (cf. also Condon and Dressel 1973; de Bruyn 1976). Variability can be induced by either clouds or shocks, which will be observed moving at approximately a constant speed, as discussed in § IV. The variability time scale should be comparable to the dynamical time scale and will thus be roughly proportional to r , and hence to λ (cf. eq. [28]).

b) Angular Structure

The analysis of VLBI observations, while still somewhat subjective, has improved over recent years as a result of more complete baseline coverage and the use of more sophisticated Fourier-inversion techniques (e.g., Readhead and Wilkinson 1978). It now appears that most sources are of the core-jet type and exhibit an unresolved bright spot at one end of an elongated structure (e.g., Wilkinson *et al.* 1977; Readhead, Cohen, and Blandford 1978; Readhead *et al.* 1978). Observed with inferior baseline coverage, these source structures are compatible with the simple symmetric double and triple models reported in earlier investigations (Cohen *et al.* 1977).

Nearly half of the strong compact radio sources appear to exhibit superluminal expansion (Cohen *et al.* 1977). The best example is 3C 345 (Seielstad *et al.* 1979) for which an expansion velocity of $(6.7 \pm 0.8)c$ ($H_0 = 55$ km s^{-1} Mpc $^{-1}$, $q_0 = 0.05$, $z = 0.595$) over a 6 year period is reported. During this time, the total angular size of the source more than doubled. Evidence has recently been presented that in some of the compact sources there is a significant rotation of the source position angle on going from the smallest to the largest angular scales (Readhead *et al.* 1978). This effect is not as yet apparent in the nuclear components of extended radio sources like Cygnus A and 3C 111 (e.g., Kellermann 1978). As pointed out by Readhead *et al.* (1978), a natural interpretation of both the rapid expansion and the bending (as well as of the absence of an observed counterjet) is possible if the brightest compact sources comprise relativistic jets whose axes make a small angle ($\sim 5^\circ$ – 10°) with the line of sight. The radio emission from the approaching component of the jet is then Doppler-brightened, and small deviations from collinearity will be exaggerated by the large projection effect. The brightest sources that we see will be those that are beamed toward us.

Nevertheless, there is a problem with this interpretation which must be overcome in any viable physical model. In order to see a systematic superluminal expansion, there must be a high relative velocity between two source components which should always be positive. However, the "emission" velocities of the two components should not be too different, for otherwise it would require an implausible coincidence to explain why the component in which the emitting material is moving faster was not considerably brighter than the slower one. In addition, if one component were not subject to relativistic beaming, then it would be difficult to explain why there were not many more bright compact sources viewed at large angles that do not exhibit large expansion velocities.

An attractive resolution of this paradox is possible in the context of the present model. Specifically, we propose that the unresolved core be identified with the innermost, optically thick region of the approaching jet, and comprise largely time-independent emission. The location of the observed core should coincide with the peak in the surface brightness of the jet, which occurs roughly where the jet becomes optically thin at the observing frequency, i.e., at a radius $r_{\text{max,ob}}(\nu) \propto \nu^{-1}$ (eq. [28]), if we adopt the assumptions of § III. The moving radio component can be identified with perhaps an accelerating cloud or a propagating shock, as described in § IV. If the component is formed inside the optically thick region of the jet, then it will not be visible at radii $r_{\text{ob}} \lesssim r_{\text{max,ob}}(\nu)$, but at larger radii it will appear to separate from the stationary component. The observed separation velocity would thus correspond to the kinematical velocity of the moving component, which may be highly relativistic ($\gamma \gg 1$), and yet the "emission" velocities of the two source components could remain comparable and also highly relativistic. In fact, as we have argued in § IV, if the variable radio emission comes from behind a moving shock, then the shock velocity must be comparable to the velocity of the jet, and this conclusion can also be deduced on dynamical grounds if the cloud or the propagating shock is observed at sufficiently large distances from its initial location. Moreover, if $\gamma \sim \gamma_j$, then the observed acceleration $cd\beta_{\text{ob}}/dt_{\text{ob}}$ will be fairly small, as is indeed observed to be the case (cf. eqs. [3]–[5] and [40]).

The fact that the two separating components have usually been observed to have comparable fluxes and surface brightnesses could be due to a selection effect resulting from the limited dynamical range and resolution of the VLBI observations. However, in our model we expect the volume emissivities as well as the sizes of the two components to be similar, so the observed emission from the core and from a shock moving with $\gamma \sim \gamma_j$ should be roughly comparable.

c) Application to 3C 345

It is clearly still premature to construct a detailed model of any particular source. However, in order to illustrate the application of the results of §§ III and IV, we consider a source like 3C 345, for which VLBI observations indicate that $\beta_{\text{ob}} \sim 7$ and $\phi_{\text{ob}} \sim 15^\circ$ (cf. Seielstad *et al.* 1979; Readhead *et al.* 1979). Since 3C 345 is one of the most rapidly expanding, as well as one of the brightest, compact extragalactic sources, we expect that both β_{ob} and \mathcal{D} are nearly maximized for this source, so we estimate that $\gamma_j \approx 7$ and $\theta \approx 8^\circ$ (cf. eqs. [1] and [6]). If we set $S_{\text{ob}} \approx 5$ Jy, $D_l \approx 4$ Gpc, $z = 0.6$, and adopt $\Lambda = 3$, $\Delta = 5$, and $k_e = 0.5$, then we deduce from equation (29) that $L \approx 1 \times 10^{46}$ ergs s $^{-1}$. Substituting this into equations (27), (28), and (30), we obtain successively $T_{\text{max}} \approx 2 \times 10^{12}$ K, $(1+z)^2 r_{\text{max,ob}}/D_l \approx 1.8\nu_9^{-1}$ milli-arcsec, and $\nu_b \approx 1.2 \times 10^{11}$ Hz. These values seem to be quite consistent with existing observations. In addition, in order to reduce the Faraday rotation estimate (eq. [32]) to $\lesssim 1$ radian, we need $F \lesssim 4 \times 10^{-5}$ or $\gamma_{e \text{ min}} \gtrsim 50$.

Consider next the fate of a "standard" emission-line cloud injected at $r_0 \sim 0.3$ pc. From equation (38) with $k_d \sim 1$ we estimate $a \approx 1.2h_{0.15}^{-1}$, and hence from equation (39) we confirm that with $n = 2$ it is possible for the cloud to be accelerated to $\gamma \approx \gamma_j \approx 7$ as long as $h_0 \lesssim 10^{14}$ cm. (This limit increases if the jet is confined.) The cloud will expand according to equation (41) to a diameter $\sim 2\pi h$, and will obstruct a reasonable fraction of the jet's area provided that $h_0 \gtrsim 10^{14}$ cm. In addition, if the cloud penetrates the jet, a further constraint is imposed by the inequalities (44). These four conditions are satisfied by h_0 in the range 10^{14} – 10^{15} cm.

Regarding the spectrum of the two major separating components in this source, our model predicts that the stationary component, which is associated with the nuclear core, should have a roughly flat spectrum and show comparatively little variability, whereas the moving component would have a variable flux which should eventually decline with a positive spectral index α . Recent VLBI measurements (Readhead *et al.* 1979; Cohen *et al.* 1979) suggest that the separating components in 3C 345, as well as in other similar sources, are indeed evolving in this manner. It therefore seems possible to account for a source like 3C 345 in terms of this general model.

d) Low-Frequency Variability

The problem of low-frequency variability has quite a long and controversial history. Recently Condon *et al.* (1979) have presented evidence to show that it is quite common in compact, flat-spectrum sources at the 20–30% level over periods of several years. The significance of these observations is that if the variability time is treated as a measure of the light crossing time of the source, then the derived brightness temperature $T_{\text{var}} = (1+z)^{-4} D_l^2 S_{\text{ob}}(\nu)/(2\nu^2 t_{\text{var}}^2 k)$ is typically 10^{14} – 10^{15} K, much greater than the Compton limit

$$T_c' \sim 10^{12}(\mathcal{D}/(1+z)\nu_{10})^{1/5} \text{ K.} \quad (46)$$

Independent evidence that the true brightness temperatures do not greatly exceed this value is provided by the apparent absence of interstellar scintillation (e.g., Condon and Dennison 1978), although intergalactic scattering might obviate this argument.

It is well known that the comoving brightness temperatures can be reduced below the Compton limit if there is relativistic expansion. Specifically, for a constant velocity source, the proper size and hence the observed transverse size of the emitting region is restricted by causality to $\sim(1+z)^{-1}\mathcal{D}ct_{\text{var}}$. The true comoving brightness temperature at the corresponding proper frequency $\nu' = \nu(1+z)/\mathcal{D}$ then satisfies

$$T_{\text{var}}(\nu) \lesssim (1+z)^{-3}\mathcal{D}^3T'(\nu(1+z)/\mathcal{D}) \lesssim (1+z)^{-3}\mathcal{D}^3T_c'. \quad (47)$$

Hence, for $\theta \lesssim \gamma^{-1}$, a thousandfold increase in apparent brightness temperature can be effected by Lorentz factors γ in the range 5–10.

However, as we showed in § II, it is possible to observe even faster variability if \mathcal{D} itself can change. For example, for a constant source with $\alpha = 0.5$, moving along a nonlinear path which is observed at an angle $\theta_0 \lesssim \gamma^{-1} \ll 1$, we can use equation (10) to show that there will be a change of $|\delta S_{\text{ob}}| = \epsilon S_{\text{ob}}$ in S_{ob} in an observed time interval $t_{\text{var}} \sim (\epsilon/3.5)(1+z)^3 R/c\gamma^3 \approx 3.3(1+z)^3 \epsilon (R/1 \text{ pc})/\gamma^3 \text{ yr}$, where R is the radius of curvature of the trajectory. The size of a coherently accelerating source is probably limited to $R/c\gamma^2$, so

$$T'(\nu(1+z)/\mathcal{D}) \gtrsim (\epsilon/3.5)^2(1+z)^3\gamma^{-3}T_{\text{var}}(\nu), \quad (48)$$

which implies that the values of γ which are needed to explain the apparent brightness temperature may in fact be smaller by a factor $(\epsilon/3.5)^{2/3}$. A similar formula holds for linear acceleration. It is apparent that with the values $\theta \sim 8^\circ$, $\gamma \sim 7$ suggested in § Vc, low-frequency variability can occur quite naturally in the strongest sources.

Unfortunately, many models that account for low-frequency variability in terms of relativistic expansion are energetically inefficient (e.g., Jones, O'Dell, and Stein 1974; Blandford and McKee 1977). This difficulty is alleviated in the case of radio emission from a relativistic jet because the radiation is beamed. To be quantitative, we can estimate the total proper internal energy of a moving source, for which the stronger inequality in (47) is satisfied, as

$$E' \gtrsim \{4\pi kT'\nu^3 t_{\text{var}}^3\} \{(1+z)t'_s/\mathcal{D}t_{\text{var}}\}, \quad (49)$$

where the braces contain, respectively, an estimate of the energy radiated and the ratio of the synchrotron cooling time t'_s (evaluated in the comoving frame) to the dynamical time. For a synchrotron source we can estimate

$$t'_s \sim 10^{11} T_{12}^{-1/3} (1+z)^{-2} \mathcal{D}^2 \nu_9^{-2} \text{ s}, \quad (50)$$

and thence calculate the total power dissipated *in the source* during the outburst to be

$$L \gtrsim E'(1+z)\mathcal{D}^{-1}t_{\text{var}}^{-1} \gtrsim 3 \times 10^{42} T_{12}^{-1/3} \nu_9 t_{\text{var}} \text{ ergs s}^{-1}, \quad (51)$$

where we measure t_{var} in years. Note that for a fixed comoving brightness temperature $T' \approx T_c'$ this expression is independent of \mathcal{D} and in fact *decreases* as the variability becomes more rapid and the observed frequency is lowered. Expression (51) is somewhat misleading, however, because it obscures the fact that \mathcal{D} must be large enough to satisfy condition (47). Nevertheless, it does demonstrate that in a source model with relativistic beaming the power requirements need not be prohibitive.

e) Polarization

In § II we discussed how the plane of polarization of an accelerating radio source can rotate rapidly without there being necessarily an accompanying large change in the total flux. This behavior appears fairly frequently in the most variable optical and radio sources, and does not seem to be attributable to changes in rotation measure (e.g., Rudnick *et al.* 1978). The best example is contained in the 1975 observations of the BL Lac object AO 0235+164, reported by Ledden and Aller (1978). In this case the swing occurred shortly after the peak of a large flux outburst and had an amplitude of $\sim 130^\circ$ and a fairly constant angular velocity. In Figure 2b we have used equation (16) to generate a fit to the data in the accelerating-cloud model of § IV. We have adopted $\gamma_j = 10$, $a = 100$, and $\theta = 5^\circ$, and have chosen $\psi = 15^\circ$, so that the swing occurs near the peak in the flux, computed under radiative assumption (i) (cf. Fig. 3); the fit was then obtained with $\eta = 5^\circ$. Of course, our choice of parameter values was quite arbitrary, and other values would yield a similar fit.

Various arguments (e.g., Ledden, Aller, and Dent 1976) suggest that this source moves relativistically and is viewed at a small angle to its velocity. According to equation (16), the large observed swing in the position angle is then consistent with the magnetic field being predominantly transverse to the velocity ($\psi \ll 1$), as expected if the magnetic field originates in the jet (cf. § III). Furthermore, in this limit ($\theta, \psi \ll 1, \beta \rightarrow 1$) the position angle of the jet should coincide with the polarization position angle roughly at midswing, so, on the basis of Figure 2b, we predict that the position angle of the putative jet in AO 0235+164 lies near $\xi = 0^\circ$.

f) Optical Observations

A small fraction of quasars ($\sim 1\%$ of optically selected and 15% of radio selected quasars) can change their optical flux by more than a magnitude in a week, and are known as optically violent variables (OVVs) (Penston and Cannon 1970; McGimsey *et al.* 1975). These objects are generally also highly active radio sources and display strong, variable, linear polarization, in contrast to the majority of quasars whose polarization appears to be very low and probably produced by scattering (Stockman and Angel 1978; Stockman 1978). OVVs are similar in many respects (apart from the prominence of emission lines) to BL Lac objects (reviewed in Stein, O'Dell, and Strittmatter 1976; Wolfe 1978).

In the light of the foregoing discussion, it seems natural to hypothesize that the sequence (radio-quiet quasars, radio-loud quasars, OVV quasars, BL Lac objects) corresponds to similar strong sources associated with relativistic jets, which are viewed at progressively decreasing angles θ to their axes (cf. Blandford and Rees 1978). The fact that several BL Lac objects appear to be surrounded by large elliptical galaxies (e.g., Miller, French, and Hawley 1978) suggests that these sources be identified with active nuclei of elliptical galaxies. In this picture, then, each nucleus comprises an isotropic, fairly steady, and unpolarized optical continuum responsible for photoionizing the emission-line gas, and in addition a variable and strongly polarized synchrotron source associated with the jet and beamed in a cone of solid angle $\sim \gamma_j^{-2}$, which in general would be larger than the solid angle subtended by the jet. Only when the observer is located within this cone does the nonthermal contribution dominate the isotropic component. BL Lacertae objects would be sources in which the Doppler boost is so large that the lines can barely be seen against the bright continuum.

If we adopt equation (11) as giving the mean observed flux and assume the constancy of R , β , r_d , and S , then $\bar{S}_{ob} \propto (1 - \beta \cos \theta)^{-(2+\alpha)}$, and the number of sources with \bar{S}_{ob} in the range $d\bar{S}_{ob}$ satisfies

$$\frac{dN}{d\bar{S}_{ob}} \propto \bar{S}_{ob}^{-(3+\alpha)/(2+\alpha)}. \quad (52)$$

That is to say, for a given population of relativistically moving sources, there will be a larger fraction of steep-spectrum sources among the beamed sources of a given \bar{S}_{ob} than among the unbeamed sources. (A similar conclusion would be reached if \bar{S}_{ob} were given instead by eq. [14], [15], or [29]). It is perhaps for this reason that BL Lac objects typically have steeper spectra than quasars. However, with a knowledge of neither the relevant luminosity function nor the distribution of Lorentz factors among sources, it is difficult to give a quantitative estimate of the ratio of beamed to unbeamed sources at a given flux.

There is some evidence that all the nonthermal emission at frequencies $\gtrsim 100$ GHz from OVVs and BL Lac objects arises in the same region (e.g., Rudnick *et al.* 1978). This too is consistent with the simple model outlined in § III, if the frequency ν_0 lies below ~ 100 GHz.

g) Relationship to Double Radio Sources

In the spirit of the above discussion it is possible to present a unified interpretation of extended double radio sources and compact, variable radio sources. We postulate that the brightest doubles (like Cygnus A) are intrinsically the brightest sources in the sky and are viewed at a large angle θ , so that their compact cores are not Doppler-boosted. The brightest compact sources (like 3C 345) then comprise the small fraction of beamed sources in the larger population of intrinsically fainter doubles. We therefore expect these compact sources to be surrounded by a low-surface-brightness, steep-spectrum radio halo, corresponding to an intermediate-power double-source component of transverse size ~ 10 – 100 kpc which is viewed along its symmetry axis. (In fact, the morphology of these halo sources need not be simply circular, because many lower-power doubles show quite complex radio structure.) There are already indications of radio halos around several compact sources, including 3C 345 (Davis, Stannard, and Conway 1977) and many BL Lac objects (Wardle 1978). Further observational support for this viewpoint may be provided by the report (Miley and Miller 1979) that $H\beta$ profiles in compact radio sources are in general simpler and narrower than in the nuclei of double radio sources. This can be understood if the line-emitting clouds in galactic nuclei and quasars are Doppler-broadened by rotation in a disk whose normal is parallel to the radio-source axis.

It will be difficult to test the hypothesis that the comparatively low-power central components of extended double sources are the unboosted counterparts of the powerful compact sources. This is because the radio-emitting electrons are unable to cool in the jet (except in its innermost parts), so the bulk of the radio flux might come from a stationary cocoon surrounding the jet, which for a similar intrinsic surface brightness would be a factor $\sim \mathcal{D}_j^{-2}(\theta \sim \pi/2) \sim \gamma^2$ brighter than the jet (cf. eq. [8]).

h) Evolutionary Considerations

The hypothesis that the brightest observed compact sources are a small subset of a larger population, highlighted by relativistic beaming toward us, has important cosmological consequences. This matter has been addressed independently by Scheuer and Readhead (1979). We defer to this paper for a discussion of the potential and

difficulties associated with the beaming hypothesis, restricting ourselves to some remarks specific to the model outlined in the present paper.

In a particular set of sources, characterized by fixed L , γ , ϕ , etc., and comprising a sufficiently large population, we expect that the viewing angle θ would be sampled well enough to test the hypothesis that relativistic beaming occurs. The variation of S_{ob} with θ for a given set of parameters depends on the model. For instance, equations (11), (14), (15) and (29) give, for flat-spectrum sources, $S_{\text{ob}} \propto (1 - \beta \cos \theta)^{-2}$, $(1 - \beta_1 \cos \theta)^{-1}$, $(1 - \beta^2 \cos^2 \theta_0)^{-3/2}$ and $(\sin \theta)^{1/6} (1 - \beta \cos \theta)^{-13/6}$, respectively, and the ranges of fluxes predicted by these models are quite different. However, it will in general be true that for every superluminal source exhibiting an expansion speed of $\beta_{\text{ob}}c$, there will be $\sim \beta_{\text{ob}}^2$ sources of lower flux, viewed from a larger angle θ . It is encouraging that there are roughly 50 times as many radio-quiet quasars as "superluminal" quasars brighter than a given optical flux, which is consistent with the value of ~ 7 for β_{ob} suggested by the VLBI observations. This hypothesis may also be tested by more sensitive searches for radio emission from the brightest radio-quiet quasars and by VLBI studies of the nuclei of the strongest extended doubles which should not exhibit expansion speeds much in excess of $2c$.

Similarly, there are at present seven low-redshift ($z \lesssim 0.1$) BL Lac objects known (Miller, French, and Hawley 1978), and this yields an estimate of $\sim 100 \text{ Gpc}^{-3}$ for their local space density, which is believed to be somewhat less than the local density of flat-spectrum radio sources of comparable brightness (e.g., Schmidt 1978). This estimated density is a fraction $\lesssim 10^{-3}$ of the density of bright elliptical galaxies, with which some BL Lac objects at least have been identified. The number of both BL Lac objects and flat-spectrum radio sources does not appear to increase as dramatically with increasing redshift as the steep-spectrum radio sources (e.g., Schmidt 1976). This cannot be explained solely in terms of geometrical beaming unless the degree of relativistic beaming itself evolves, in the sense that younger sources move with smaller Lorentz factors.

VI. CONCLUSIONS

We have presented a general model for compact radio sources in which the radio emission (together with non-thermal radiation at high frequencies) is presumed to originate from a collimated relativistic jet. Temporal and spatial variability may be attributed to the motion of individual density inhomogeneities within the outer parts of the jet.

The following observed features find an explanation in this model: (i) the flat radio spectra and steep optical spectra associated with quasars; (ii) superluminal expansion and flux variability; (iii) rapid swings in polarization angle; (iv) the relationship between radio-quiet quasars, radio-loud quasars, OVVs, and BL Lac objects; (v) the relative weakness of the central components of the powerful extended double sources.

If our classification of these objects is largely determined by our orientation with respect to the jet direction, then the following general observational tests are suggested: (i) Weak, steep-spectrum radio halos should be found surrounding the most powerful variable radio sources. (ii) Powerful compact radio sources should be strongly asymmetrical and may frequently display rotation of the source position angle and superluminal expansion. (iii) The relatively weak central components of the powerful doubles like Cygnus A should be more symmetrical and better aligned with the outer components, and not show observed expansion velocities larger than $\sim 2c$.

Predictions relevant to specific objects like 3C 345 and AO 0235+164 can also be made.

The authors thank A. Readhead and M. Rees for discussions and encouragement and T. Jones for helpful comments on the manuscript. Hospitality at the Santa Cruz Summer Workshop on Quasars and Active Galactic Nuclei (R. B. and A. K.) and the Institute of Astronomy, Cambridge (facilitated by a grant from the NATO Scientific Affairs Division) (R. B.), is gratefully acknowledged.

REFERENCES

- Blandford, R. D., and Königl, A. 1979, *Ap. Letters*, **20**, 15.
 Blandford, R. D., and McKee, C. F. 1977, *M.N.R.A.S.*, **180**, 343.
 Blandford, R. D., McKee, C. F., and Rees, M. J. 1977, *Nature*, **267**, 211.
 Blandford, R. D., and Rees, M. J. 1978, in *Pittsburgh Conference on BL Lac Objects*, ed. A. M. Wolfe (Pittsburgh: University of Pittsburgh), p. 328.
 Brandie, G. W., Bridle, A. H., and Kesteven, M. J. L. 1974, *Nature*, **252**, 212.
 Burch, S. F. 1977, *M.N.R.A.S.*, **181**, 599.
 Christiansen, W. A., and Scott, J. S. 1977, *Ap. J. (Letters)*, **216**, L1.
 Christiansen, W. A., Scott, J. S., and Vestrand, W. T. 1978, *Ap. J.*, **223**, 13.
 Cohen, M. H., et al. 1977, *Nature*, **268**, 405.
 Cohen, M. H., Pearson, T. J., Readhead, A. C. S., Seielstad, G. A., Simon, R. S., and Walker, R. C. 1979, *Ap. J.*, **231**, 293.
 Condon, J. J., Balonek, T. J., and Jauncey, D. L. 1975, *Ap. J.*, **80**, 887.
 Condon, J. J., and Dennison, B. 1978, *Ap. J.*, **224**, 835.
 Condon, J. J., and Dressel, L. L. 1973, *Ap. Letters*, **15**, 203.
 Condon, J. J., Ledden, J. E., O'Dell, S. L., and Dennison, B. 1979, *A.J.*, **84**, 1.
 Davis, R. J., Stannard, D., and Conway, R. G. 1977, *Nature*, **267**, 596.
 de Bruyn, A. G. 1976, *Astr. Ap.*, **52**, 439.
 De Young, D. S. 1976, *Ann. Rev. Astr. Ap.*, **14**, 447.
 De Young, D. S., and Axford, W. I. 1967, *Nature*, **216**, 129.
 Ferguson, D. C. 1971, *Nature Phys. Sci.*, **234**, 86.
 Hunstead, R. W. 1972, *Ap. Letters*, **12**, 193.
 Jones, T. W., and O'Dell, S. L. 1977, *Astr. Ap.*, **61**, 291.
 Jones, T. W., O'Dell, S. L., and Stein, W. A. 1974, *Ap. J.*, **192**, 261.
 Jones, T. W., and Tobin, W. 1977, *Ap. J.*, **215**, 474.
 Kellermann, K. I. 1966, *Ap. J.*, **146**, 621.
 ———. 1978, *Physica Scripta*, **17**, 257.
 Kellermann, K. I., and Pauliny-Toth, I. I. K. 1969, *Ap. J. (Letters)*, **155**, L71.

- Ledden, J. E., and Aller, H. D. 1978, in *Pittsburgh Conference on BL Lac Objects*, ed. A. M. Wolfe (Pittsburgh: University of Pittsburgh), p. 60.
- Ledden, J. E., Aller, H. D., and Dent, W. A. 1976, *Nature*, **260**, 752.
- Marscher, A. P. 1978, *Ap. J.*, **219**, 392.
- McGimsey, B. Q., et al. 1975, *A.J.*, **80**, 895.
- Miley, G. K., and Miller, J. S. 1979, *Ap. J. (Letters)*, **228**, L55.
- Miller, J. S., French, H. B., and Hawley, S. A. 1978, in *Pittsburgh Conference on BL Lac Objects*, ed. A. M. Wolfe (Pittsburgh: University of Pittsburgh), p. 176.
- O'Dell, S. L. 1978, in *Pittsburgh Conference on BL Lac Objects*, ed. A. M. Wolfe (Pittsburgh: University of Pittsburgh), p. 312.
- Osterbrock, D. E. 1978, *Physica Scripta*, **17**, 285.
- Penston, M. V., and Cannon, R. D. 1970, *R. Obs. Bull.*, **159**, 85.
- Readhead, A. C. S., Cohen, M. H., and Blandford, R. D. 1978, *Nature*, **272**, 131.
- Readhead, A. C. S., Cohen, M. H., Pearson, T. J., and Wilkinson, P. N. 1978, *Nature*, **276**, 768.
- Readhead, A. C. S., Pearson, T. J., Cohen, M. H., Ewing, M. S., and Moffett, A. T. 1979, *Ap. J.*, **231**, 299.
- Readhead, A. C. S., and Wilkinson, P. N. 1978, *Ap. J.*, **223**, 25.
- Rees, M. J. 1978, *M.N.R.A.S.*, **184**, 61.
- Rudnick, L., Owen, F. N., Jones, T. W., Puschell, J. J., and Stein, W. A. 1978, *Ap. J. (Letters)*, **225**, L5.
- Scheuer, P. A. G., and Readhead, A. C. S. 1979, *Nature*, **277**, 182.
- Schmidt, M. 1976, *Ap. J. (Letters)*, **209**, L55.
- . 1978, *Physica Scripta*, **17**, 135.
- Seielstad, G. A., Cohen, M. H., Linfield, R. P., Moffett, A. T., Romney, J. D., Schilizzi, R. T., and Shaffer, D. B. 1979, *Ap. J.*, **229**, 53.
- Shields, G. A. 1978, in *Pittsburgh Conference on BL Lac Objects*, ed. A. M. Wolfe (Pittsburgh: University of Pittsburgh), p. 257.
- Sramek, R. A., and Weedman, D. W. 1978, *Ap. J.*, **221**, 468.
- Stein, W. A., O'Dell, S. L., and Strittmatter, P. A. 1976, *Ann. Rev. Astr. Ap.*, **14**, 173.
- Stockman, H. S. 1978, in *Pittsburgh Conference on BL Lac Objects*, ed. A. M. Wolfe (Pittsburgh: University of Pittsburgh), p. 149.
- Stockman, H. S., and Angel, J. R. P. 1978, *Ap. J. (Letters)*, **220**, L67.
- Usher, P. D. 1975, *Ap. J. (Letters)*, **198**, L57.
- Waggett, P. C., Warner, P. J., and Baldwin, J. E. 1977, *M.N.R.A.S.*, **181**, 465.
- Wall, J. V. 1975, *Observatory*, **95**, 196.
- Wardle, J. F. C. 1977, *Nature*, **269**, 563.
- . 1978, in *Pittsburgh Conference on BL Lac Objects*, ed. A. M. Wolfe (Pittsburgh: University of Pittsburgh), p. 39.
- Wilkinson, P. N., Readhead, A. C. S., Purcell, G. H., and Anderson, B. 1977, *Nature*, **269**, 764.
- Wolfe, A. M. (ed.) 1978, *Pittsburgh Conference on BL Lac Objects* (Pittsburgh: University of Pittsburgh).

ROGER D. BLANDFORD and ARIEH KÖNIGL: Bridge Annex 130-33, California Institute of Technology, Pasadena, CA 91125